NANO LETTERS

pubs.acs.org/NanoLett Letter

Epitaxial Stabilization of a Pyrochlore Interface between Weyl Semimetal and Spin Ice

Mikhail Kareev, Xiaoran Liu, Michael Terilli, Fangdi Wen, Tsung-Chi Wu, Dorothy Doughty, Hongze Li, Jianshi Zhou, Qinghua Zhang, Lin Gu, and Jak Chakhalian

Cite This: *Nano Lett.* 2025, 25, 966−972 Read Online

ACCESS | Metrics & More | Article Recommendations | Supporting Information

ABSTRACT: Pyrochlore materials are known for their exotic magnetic and topological phases arising from complex interactions among electron correlations, band topology, and geometric frustration. Interfaces between different pyrochlore crystals characterized by complex many-body ground states hold immense potential for novel interfacial phenomena due to the strong interactions between these phases. However, the realization of such interfaces has been severely hindered by limitations in material synthesis methods. In this study, we discover a robust synthesis method that produces the previously unexplored epitaxial pyrochlore interface between spin ice $Dy_2Ti_2O_7$ and Weyl semimetal $Eu_2Ir_2O_7$. The method relies on an ultrahigh supersaturation regime during deposition aided by directional IR-laser-driven thermal gradients, transforming amorphous covalent networks into nearly perfectly ordered, atomically sharp interfaces with a chemically ideal arrangement of ions. The novel pyrochlore interface enables the study of interactions between relativistic Weyl fermions and spin ice magnetic monopoles, opening a path to designing diverse pyrochlore interfaces.

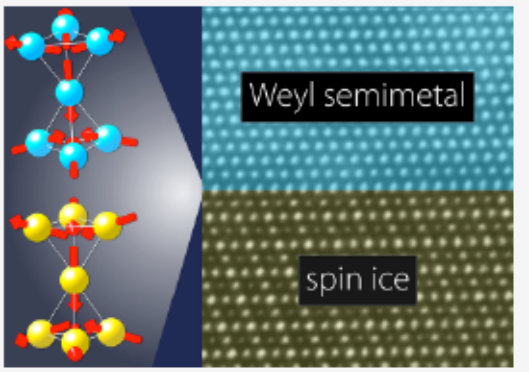

KEYWORDS: *pyrochlore interfaces, spin ice, Weyl semimetal, frustrated magnetism, topological quantum materials, thin-film synthesis*

Interface-driven phenomena have been pivotal in advancing the frontier of condensed matter physics to offer novel insights into the unusual properties of quantum materials. Fundamental discoveries, such as the integer and fractional quantum Hall effects observed in two-dimensional electron systems at semiconductor interfaces, illustrate the impact of reduced dimensionality and strong electron−electron interactions in engineered interfaces.[1−5] Interfaces also open opportunities for the modulation of exotic electronic properties through the deliberate combination of layers with antagonistic orders (e.g., superconductivity and ferromagnetism).[6,7] Today, interface-engineered artificial quantum structures can help challenge the existing paradigms in solids and deliver the promise of novel emergent quantum phenomena.[8−11]

Interface engineering is especially intriguing in the case of lattice systems which host many exotic phenomena, such as the -pyrochlores, characterized by the formula $A_2B_2O_7$. Here, A denotes a rare-earth element (Pr···Lu), and B represents a platinum group metal (e.g., Rh, Pd, Os, Ir, Pt) or 3d ions (e.g., Zn, Ti). This family exhibits a unique crystal structure of corner-sharing tetrahedra, creating a highly frustrated lattice for both A and B ions.[12−15] Such a topological motif enforces magnetic frustration and ground-state spin degeneracy. Combined with the strong spin−orbit interaction characteristic of the 5d platinum group ions, the pyrochlore family is predicted to host novel exotic quantum states, such as spin liquids, magnetic monopole crystals, fractionalized magnetic moments, and topologically protected magnetic modes.[16−21] Those exotic states are of fundamental interest for basic physics and potential applications in quantum spintronics.[10,22−27] When engineered into oriented interfaces, the vast array of topological and magnetic properties in pyrochlores make these artificial structures exceptionally promising for exploring the interplay between those states to unveil the emergent exotic phenomena.

To illustrate this approach, we consider the spin ice pyrochlore titanate, $A_2Ti_2O_7$,[9,28−31] and pyrochlore iridate (PyIr), $A_2Ir_2O_7$. The titanates subgroup of pyrochlores is characterized by magnetically silent Ti-sites and magnetically active A-sites (e.g., Dy), which harbor strong spin frustration due to the "two spin in−two spin out" (2i-2o) rule, i.e., a local constraint imposed on the magnetic moments within the pyrochlore lattice (see Figure 1a). The effect of magnetic frustration can lead to a unique quantum spin-disordered state, marked by Coulomb correlations. Within this state, the

Received: August 16, 2024
Revised: December 5, 2024
Accepted: December 6, 2024
Published: January 2, 2025

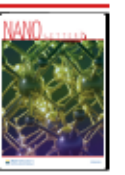

https://doi.org/10.1021/acs.nanolett.4c03969
Nano Lett. 2025, 25, 966−972

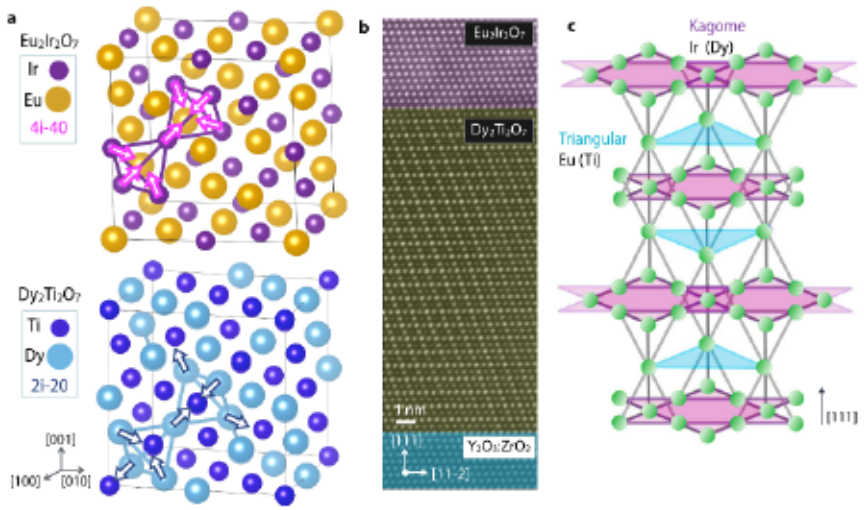

Figure 1. (a) Cation (A-site and B-site) sublattices of the pyrochlore phase with the superimposed 4i-4o and 2i-2o spin structures, respectively. (b) HAADF-STEM atomic columns mapping of PyIr/PyTi heterostructure and YSZ substrate viewed along the $[1\bar{1}0]$ projection. (c). When viewed along the [111] direction, the crystal structure forms alternating kagome and triangular atomic planes, which imposes strong geometric frustration in the [111]-oriented thin film.

concepts of emergent "magnetic monopole" entwined by Dirac strings and U(1) photon-like excitations have gathered large theoretical and experimental interest.[28,29,32] In PyIr, the Ir sites are magnetically active and follow "four spin in−four spin out" (4i-4o) configuration (Figure 1a); this system harbors topologically nontrivial phases, such as chiral spin liquid, axion insulator, and Weyl semimetal.[28,33−37]

Tailor-made, high-quality interfaces of these pyrochlore quantum materials are a new exciting venue. In particular, the iridate/titanate heterostructure has been theorized to host a two-dimensional (2D) monopole gas at the interface.[10,16,18,31] However, to date, there has been no clearly established path for realizing these high-quality heterostructures.

In this Letter, we report on the discovery of a new approach for creating high-quality pyrochlore heterostructures exemplified by the atomically sharp interface between the spin ice titanate $Dy_2Ti_2O_7$ (DTO) and magnetic Weyl semimetal $Eu_2Ir_2O_7$ (EIO).

We confirm the power of the new synthesis method to form an atomically sharp interface between the spin-ice and Weyl semimetal by thorough scanning transmission electron microscopy (STEM) imaging, high-angle annular dark field (HAADF), and electron energy loss spectroscopy (EELS) analysis. Moreover, our protocol remarkably improves the surface quality, as verified by X-ray reflectivity and atomic force microscopy (AFM) measurements. This discovery opens exciting opportunities for in-depth experimental exploration of the novel topological and magnetic states inherent to the pyrochlore family and significantly expands the material's space en route to synthetic quantum matter.

While the layer-by-layer growth of pyrochlore titanates (spin ice) has been recently achieved,[38−40] creating -pyrochlores of the Group VIIIb metals (e.g., Os, Ir, Pt) poses tough challenges. In particular, the in-situ growth of pyrochlore iridate (PyIr) artificial structures is impeded by the very low reactivity of Ir and the tendency for the formation of gaseous volatile species as IrO_3 under high temperatures and O_2 pressures.[41] To navigate these challenges, several creative strategies have been tried, including physical vapor deposition (PVD) with cosputtering of IrO_2,[42−44] flash annealing methods.[23,45,46] and solid-phase epitaxy (SPE);[47,48] the latter notably offers a route for in-situ growth of epitaxial pyrochlore thin films and heterostructures.[49] In our new method, a unique combination of SPE and epitaxial growth conducted at the limit of extreme supersaturation by pulsed laser deposition (PLD) enables precise control over the atomic structure and valence state of cations in the heterostructure of different pyrochlore layers.

In the spirit of rational materials design, a template buffer layer (DTO) is deposited on the YSZ substrate for the SPE of EIO in a layer-by-layer way with subunit cell precision as described in refs 39 and 40 (also see Figure 2b). In what follows, we present a comprehensive description of our new experimental design for the hybrid SPE/PLD method illustrated in Figures 2a−c. In step (i), the amorphous layer thickness is meticulously calibrated by adjusting the UV-laser pulse rate (see Table S2). In step (ii), the SPE-driven crystallization from the amorphous state proceeds on the atomically flat pyrochlore DTO template. Remarkably, such a two-stage annealing protocol prevents the formation of IrO_3 volatile gas at elevated oxygen pressures. As a result, an amorphous metastable pyrochlore matrix free from iridium deficiencies can be formed.[49,50] Finally, in step (iii), the amorphous iridate layer undergoes the IR-laser-controlled post-annealing. Extensive X-ray diffraction characterization shows that the post-annealing duration is a critical tuning parameter: short post-annealing intervals result in a highly heterogeneous mixture of crystalline and amorphous phases (see Figure S3).

As shown in Figures 2d−g, during the deposition phase, reflection high-energy electron diffraction (RHEED) imaging reveals broad rings, demonstrating short-range atomic order within the amorphous pyrochlore layer.[51] Although RHEED monitoring is infeasible during the high-pressure annealing step conducted in ∼500 Torr of O_2 gas, the post-annealing RHEED images clearly exhibit a characteristic streaky pattern, confirming the formation of high-quality long-range crystalline order. The resulting new heterostructure is compatible with the application of nanolithographic methods and surface-sensitive analytical techniques, such as angle-resolved photo-

https://doi.org/10.1021/acs.nanolett.4c03969
Nano Lett. 2025, 25, 966−972

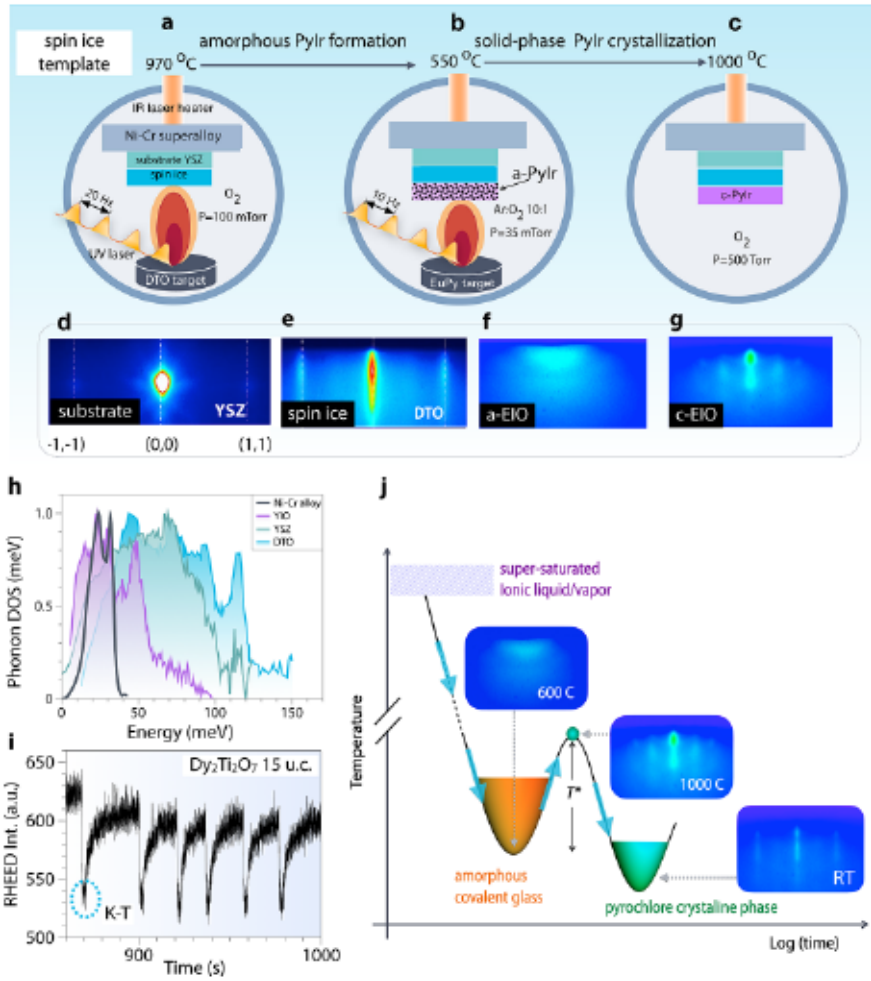

Figure 2. Pyrochlore iridate in situ two-stage fabrication sequence. (a) A DTO layer grown in a layer-by-layer way by PLD on YSZ. (b) Deposition of the amorphous EIO pyrochlore layer, followed by (c) SPE at a high-temperature annealing synthesis cycle by an infrared (IR) laser. (d)−(g) In situ RHEED images of the YSZ substrate and each subsequent phase of the growth. (h) Phonon DOS for all constituents, including Ni−Cr alloy adsorber, substrate, and heterostructure. Adapted from ref 67, available under a CC-BY 4.0 license (Copyright 2022, Springer Nature), and with permission from refs 68−70 (Copyright 2024, American Physical Society). (i) RHEED intensity oscillations during the DTO growth. A single wiggle corresponds to a kagome-triangular slab or 1/2 unit cell. (j) Kinetically stabilized growth regimes. Ultrafast quenching of the amorphous iridate film at the pre-SPE stage into a metastable supercooled liquid (glass state). The consequent devitrification of the random continuous glassy network leads to the formation of a pyrochlore iridate film with excellent electronic and chemical properties.

electron spectroscopy and scanning tunneling microscopy, crucial for probing topological properties (e.g., the edge states).

Commonly, in SPE, the post-annealing is executed ex-situ in a high-temperature furnace. This process is naturally characterized by a highly nonuniform distribution and propagation of heat throughout the sample. In sharp contrast, our new all-in situ IR-laser annealing places the YSZ substrate's backside in direct contact with a planar heat absorber composed of Inconel, a Ni−Cr superalloy (see the Supporting Information (Figure S8)). We propose that this unique IR-laser instrumentation integrated into the PLD growth chamber facilitates controlled heat propagation from the substrate across the interfaces toward the surface.[52,53] In addition, as recently demonstrated in ref 54 the phonon density of state (DOS) overlap between DTO and crystalline EIO suggests minimal interfacial thermal resistance, facilitating remarkably efficient heat transport across the interface during annealing (Figure 2h), critical for the rapid recrystallization of the amorphous EIO layer into a pyrochlore structure.

To further illuminate the microscopic details of our PLD/SPE growth mechanism, we consider the growth kinetics during the formation of the amorphous network and how it converts into a pyrochlore crystal. First, we note that SPE itself involves the ordering of atoms from a metastable amorphous phase into a crystalline structure through local bond rearrangements at the moving crystalline−amorphous interface all occurring in the solid phase.[55] Extensive previous RHEED studies on perovskite oxides grown by SPE reveal how crystallization progresses through the thermally activated movement of the crystalline/amorphous interface.[56] These findings can also be translated into a consistent mechanism underlying the pyrochlore iridate layer growth. Initially, the EIO layer represents a kinetically stabilized, metastable amorphous ionic network or covalent glass with highly anisotropic bonds due to the nature of 5d- and 5f-orbitals involved, wherein the molecular disorder and the thermodynamic properties akin to the undercooled melt are frozen. The transformation process is illustrated in Figure 2j. During the iridate layer deposition, ultrafast cooling (quenching) prevents

https://doi.org/10.1021/acs.nanolett.4c03969
Nano Lett. 2025, 25, 966−972

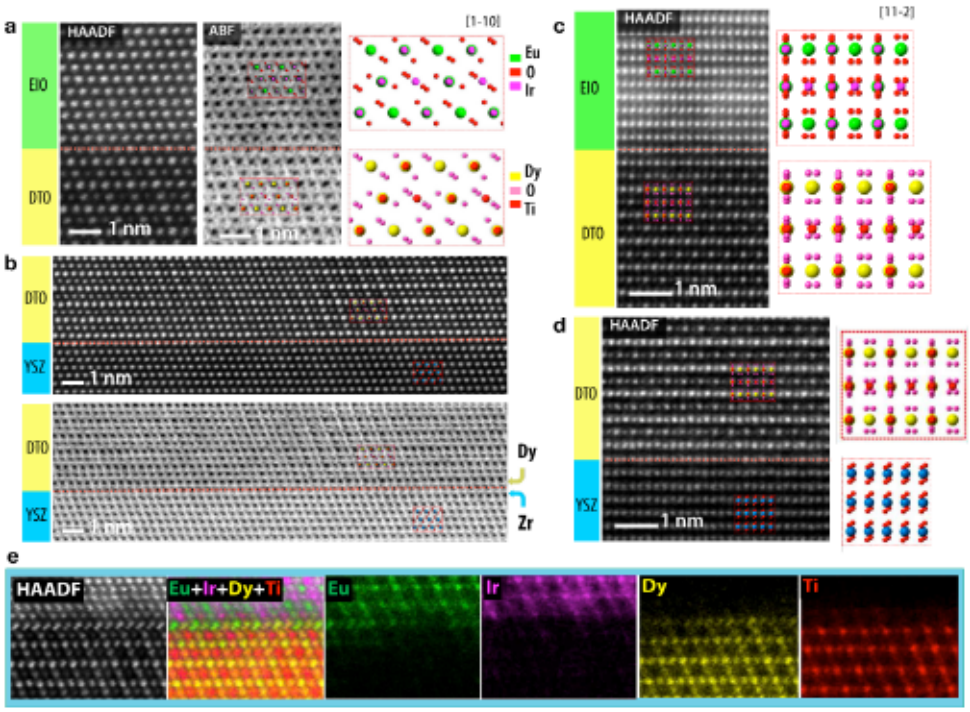

Figure 3. Atomically resolved HAADF and ABF-STEM survey images to identify the oxygen sublattice along the (a, b) [1$\bar{1}$0] and (c, d) [11$\bar{2}$] projections. A schematic illustrates stacking sequences at the Py-Py (EIO−DTO) and Py-Fl (DTO-YSZ) interfaces along the [11$\bar{2}$] and [1$\bar{1}$0] projections. (e) Left to right: STEM-EELS atomic column mapping of the EIO and DTO interfaces along with the HAADF-STEM survey image, composite color maps of the local concentration combined and the individual constituent ions identified in the layers; color coded as Eu (green), Ir (magenta), Dy (yellow), and Ti (red).

nucleation, maintaining its metastable amorphous state. Subsequent devitrification of this random continuous network yields a pyrochlore iridate structure of superior crystallinity.[57]

Finally, we highlight the specific condition during the *interrupted* PLD process that prevents premature unwanted crystallization.[39,40,49,58,59] As shown in Figure 2j, adopting the special interrupted PLD mode under extreme supersaturation and fast flux modulation provides precise kinetic control, effectively postponing the onset of crystallization.[58] The formation of an amorphous iridate layer is achieved through ultrafast quenching in the ionic-liquid phase and further suppresses crystallization and induces a kinetically stabilized supercooled liquid state.[60] In the SPE stage, we also employ a nonlinear cooling regime with rapid cooling at higher temperatures until the minimum nucleation threshold is reached, followed by a slower cooling rate at lower temperatures to accommodate the increasing relaxation time of the supercooled liquid created in the PLD stage (see Figure S9 and Table S3 for a full temperature ramping profile). Notably, our control experiments with a constant cooling rate result in premature crystallization at the DTO/EIO interface and a low-quality, defective iridate layer,[54,61,62] signifying the important role of the ultrafast quenching.

To confirm that the discovered SPE/PLD growth mode yields high-quality structures with atomically flat surfaces/interfaces, we conducted detailed STEM-EELS and HAADF-ABF (annular bright-field) measurements and analyses. Post-annealing examinations shown in Figure 3 demonstrate the absence of the amorphous phase, as evident in atomically resolved HAADF and ABF images. The pyrochlore phase, the A-site (Dy, Eu) and B-site (Ti, Ir) cation sublattices, and the kagome-triangular sequence are visualized by elemental mapping obtained from the detailed STEM-EELS analysis. Additionally, anion (oxygen) sublattice motifs are distinctly visible in the ABF images; atomic structure models are superimposed on these ABF images to identify the oxygen sublattice across the [1$\bar{1}$0] and [11$\bar{2}$] projections (Figures 3a–d, respectively). In addition, as shown in Figure 3c, the stacking sequence at both the EIO−DTO and DTO-YSZ interfaces is readily identified in HAADF-ABF images along the [11$\bar{2}$] and [1$\bar{1}$0] projections, corroborated by the ABF analysis reported in ref 63.

A direct comparison of HAADF vs ABF imaging reveals that the oxygen sublattices at the EIO/DTO interface are continuous and identical (Figure 3c). Assuming a conventional solid-state reaction mechanism, one would expect to observe intermixing due to the diffusion of the Eu_2O_3 and IrO_2 components as the pyrochlore phase forms. Remarkably, in our heterostructure, the intermixing at the EIO−DTO interface is strictly confined to one or two atomic planes, a statement supported by elemental mapping shown in Figure 3a. In addition, the ABF imaging of the DTO/YSZ interface, shown in Figure 3, implies that the oxygen sublattices are in a close registry between DTO (pyrochlore) and YSZ (fluorite).

Next, we turn our attention to the surface structural properties. For this purpose, we evaluated the surface roughness of both single-layered $Eu_2Ir_2O_7$ samples and bilayered EIO/DTO samples, presented in Table S1 in the Supporting Information. The surface roughness is quantified for all samples using low-angle X-ray reflectivity (XRR) measurements, which are modeled to extract the roughness parameters. First, we note that the bilayer growth on DTO markedly improves the surface roughness compared to the single-layer films. In particular, the critical-angle reflected

https://doi.org/10.1021/acs.nanolett.4c03969
Nano Lett. 2025, 25, 966−972

intensity is significantly higher for the bilayer films, indicating a flatter surface with a roughness reduction of over 50%. Furthermore, atomic force microscopy (AFM) scans are taken on both sets of samples in a 1.5 μm × 1.5 μm field of view to obtain a 2D real-space measurement of the surface roughness. These measurements reveal an even more drastic difference in the surface roughness, where an Sq value is five times lower in bilayer EIO/DTO compared to the single-layer counterparts. The combined XRR and AFM measurements affirm the remarkably flatter surface and interface achieved by our new PLD/SPE method.

Here, we remark on the reasons for the DTO layer's contribution to the flatness of the surface and interfaces. Unlike the fluorite structure of the YSZ substrate, which randomly hosts vacancies at one-eighth of the oxygen sites, the pyrochlore−pyrochlore DTO/EIO interface ensures a complete anion (oxygen) sublattice matching and fosters immediate nucleation at a submicroscopic level. Additionally, the atomic precision achieved in the layer-by-layer growth of DTO yields an atomically flat interface, promoting a remarkably smoother iridate layer crystallized in the vicinity of the interface.[55] The flatness of the interface propagates throughout the iridate layer during the SPE crystallization process, leading to a very low surface/interface roughness.[64] Compared to the recent report on the growth of a non-rare-earth $Bi_2Ir_2O_7$ pyrochlore paramagnetic metal on a DTO bulk single crystal,[65] our heterostructure comprised of DTO thin films reveals a high-quality interface free from the deposition anomalies associated with the substrate surface defects and deformations.

In conclusion, we unveil a growth method that facilitates the creation of exceptionally high-quality oriented pyrochlore heterointerfaces. This technique has been successfully applied to fabricate a unique interface between spin ice titanate $Dy_2Ti_2O_7$ (DTO) and magnetic Weyl semimetal iridate $Eu_2Ir_2O_7$ (EIO), forming an unexplored type of artificial quantum matter where the relativistic Weyl fermions interact with magnetic monopole excitations of the spin ice.[66] The resulting heterostructures have excellent stoichiometry, high crystallinity, a nanoscale-level flat surface, and interface qualities surpassing previously reported methods. The strategy established here opens exciting new avenues for creating novel interfaces, expanding our materials toolkit toward synthetic quantum architectures with emergent physical properties unattainable in bulk crystals.

METHODS

The pyrochlore iridate targets were ablated using a KrF excimer laser (λ = 248 nm, energy density 3 J/cm^2) at a repetition rate of 10 Hz. The deposition was carried out at a low substrate temperature of 550 °C, under a 35 mTorr atmosphere of a mixture of Ar and O_2 gases (partial pressure ratio, Ar: O_2 = 10:1). The film was post-annealed inside the chamber at 1050 °C, under a 500 Torr atmosphere of pure O_2 (30 min for Eu, <20 min for Y), and then cooled to room temperature. A detailed description of spin ice growth can be found elsewhere.[39,40] An X-ray diffractometer (Malvern Panalytical Empyrean) was used to characterize the reciprocal space of the sample and to understand the film's crystal structure to obtain (1) X-ray reflectivity (XRR) and (2) X-ray diffraction [XRD, reciprocal space map (RSM)] data. High-angle annular dark-field (HAADF) and annular-bright-field (ABF) imaging were performed in the STEM mode using a JEOL JEM ARM 200CF microscope at the Institute of Physics, Chinese Academy of Sciences.

ASSOCIATED CONTENT

Supporting Information

The Supporting Information is available free of charge at https://pubs.acs.org/doi/10.1021/acs.nanolett.4c03969.

Additional experimental details (PDF)

AUTHOR INFORMATION

Corresponding Authors

Mikhail Kareev − *Department of Physics and Astronomy, Rutgers University, Piscataway, New Jersey 08854, United States;* orcid.org/0009-0001-8838-5608; Email: mk1517@physics.rutgers.edu

Jak Chakhalian − *Department of Physics and Astronomy, Rutgers University, Piscataway, New Jersey 08854, United States;* Email: jak.chakhalian@rutgers.edu

Authors

Xiaoran Liu − *Beijing National Laboratory for Condensed Matter Physics and Institute of Physics, Chinese Academy of Sciences, Beijing 100190, China;* orcid.org/0000-0003-0938-6109

Michael Terilli − *Department of Physics and Astronomy, Rutgers University, Piscataway, New Jersey 08854, United States*

Fangdi Wen − *Department of Physics and Astronomy, Rutgers University, Piscataway, New Jersey 08854, United States;* orcid.org/0000-0003-2314-8561

Tsung-Chi Wu − *Department of Physics and Astronomy, Rutgers University, Piscataway, New Jersey 08854, United States*

Dorothy Doughty − *Department of Physics and Astronomy, Rutgers University, Piscataway, New Jersey 08854, United States*

Hongze Li − *Department of Mechanical Engineering, University of Texas at Austin, Austin, Texas 78712, United States;* orcid.org/0000-0002-3017-383X

Jianshi Zhou − *Department of Mechanical Engineering, University of Texas at Austin, Austin, Texas 78712, United States;* orcid.org/0000-0002-7667-5640

Qinghua Zhang − *Beijing National Laboratory for Condensed Matter Physics and Institute of Physics, Chinese Academy of Sciences, Beijing 100190, China*

Lin Gu − *Beijing National Center for Electron Microscopy and Laboratory of Advanced Materials, Department of Materials Science and Engineering, Tsinghua University, Beijing 100084, China*

Complete contact information is available at: https://pubs.acs.org/10.1021/acs.nanolett.4c03969

Notes

The authors declare no competing financial interest.

ACKNOWLEDGMENTS

M.K., M.T., F.W., T.-C.W., D.D., and J.C. acknowledge the support by the U.S. Department of Energy, Office of Science, Office of Basic Energy Sciences, under Award No. DE-SC0022160. X.L. acknowledges the support of the National Natural Science Foundation of China (Grant No. 12204521) and the National Key R&D Program of China (Grant No.

2022YFA1403400). H.L. and J.Z. acknowledge the support from NSF Grant Nos. DMR-1720595 and DMR-2308817. Q.Z. and L.G. acknowledge the support of the National Natural Science Foundation of China (Nos. 52250402, 52025025, and 52072400) and the National Key R&D Program of China (Grant No. 2024YFA1409500).

REFERENCES

(1) Peraticos, E.; Kumar, S.; Pepper, M.; Siddiki, A.; Farrer, I.; Ritchie, D.; Jones, G.; Griffiths, J. Resistance hysteresis in the integer and fractional quantum Hall regime. *Phys. Rev. B* **2023**, *107*, 205307.
(2) Park, H.; et al. Observation of fractionally quantized anomalous Hall effect. *Nature* **2023**, *622*, 74−79.
(3) Xu, F.; Sun, Z.; Jia, T.; Liu, C.; Xu, C.; Li, C.; Gu, Y.; Watanabe, K.; Taniguchi, T.; Tong, B.; et al. Observation of integer and fractional quantum anomalous Hall effects in twisted bilayer $MoTe_2$. *Phys. Rev. X* **2023**, *13*, 031037.
(4) Cheng, G.; Tomczyk, M.; Tacla, A. B.; Lee, H.; Lu, S.; Veazey, J. P.; Huang, M.; Irvin, P.; Ryu, S.; Eom, C.-B.; et al. others Tunable electron-electron interactions in $LaAlO_3/SrTiO_3$ nanostructures. *Phys. Rev. X* **2016**, *6*, 041042.
(5) Papic, Z.; Balram, A. C. In *Encyclopedia of Condensed Matter Physics*, Second Edition; Chakraborty, T., Ed.; Academic Press: Oxford, 2024; pp 285−307.
(6) Chakhalian, J.; Freeland, J. W.; Srajer, G.; Strempfer, J.; Khaliullin, G.; Cezar, J. C.; Charlton, T.; Dalgliesh, R.; Bernhard, C.; Cristiani, G.; Habermeier, H.-U.; Keimer, B. Magnetism at the interface between ferromagnetic and superconducting oxides. *Nat. Phys.* **2006**, *2*, 244−248.
(7) Prajapat, C. L.; Singh, S.; Bhattacharya, D.; Ravikumar, G.; Basu, S.; Mattauch, S.; Zheng, J.-G.; Aoki, T.; Paul, A. Proximity effects across oxide-interfaces of superconductor-insulator-ferromagnet hybrid heterostructure. *Sci. Rep.* **2018**, *8*, 3732.
(8) Liu, J.; Kargarian, M.; Kareev, M.; Gray, B.; Ryan, P. J.; Cruz, A.; Tahir, N.; Chuang, Y.-D.; Guo, J.; Rondinelli, J. M.; Freeland, J. W.; Fiete, G. A.; Chakhalian, J. Heterointerface engineered electronic and magnetic phases of $NdNiO_3$ thin films. *Nat. Commun.* **2013**, *4*, 2714.
(9) Ohno, M.; Fujita, T. C.; Kawasaki, M. Proximity effect of emergent field from spin ice in an oxide heterostructure. *Sci. Adv.* **2024**, *10*, No. eadk6308.
(10) Zhang, B.; Lu, P.; Tabrizian, R.; Feng, P. X.-L.; Wu, Y. 2D Magnetic heterostructures: spintronics and quantum future. *npj Spintronics* **2024**, *2*, 6.
(11) Ahn, E. C. 2D materials for spintronic devices. *npj 2D Mater. Appl.* **2020**, *4*, 17.
(12) Gardner, J. S.; Gingras, M. J.; Greedan, J. E. Magnetic pyrochlore oxides. *Rev. Mod. Phys.* **2010**, *82*, 53.
(13) Rau, J. G.; Gingras, M. J. Frustrated Quantum Rare-Earth Pyrochlores. *Ann. Rev. Condensed Matter Phys.* **2019**, *10*, 357−386.
(14) Hallas, A. M.; Gaudet, J.; Gaulin, B. D. Experimental Insights into Ground-State Selection of Quantum XY Pyrochlores. *Ann. Rev. Condensed Matter Phys.* **2018**, *9*, 105−124.
(15) Rau, J. G.; Lee, E. K.-H.; Kee, H.-Y. Spin-Orbit Physics Giving Rise to Novel Phases in Correlated Systems: Iridates and Related Materials. *Ann. Rev. Condensed Matter Phys.* **2016**, *7*, 195−221.
(16) Miao, L.; Lee, Y.; Mei, A. B.; Lawler, M. J.; Shen, K. M. Two-dimensional magnetic monopole gas in an oxide heterostructure. *Nat. Commun.* **2020**, *11*, 1341.
(17) Khomskii, D. I. Electric dipoles on magnetic monopoles in spin ice. *Nat. Commun.* **2012**, *3*, 904.
(18) Khomskii, D. I. Electric activity at magnetic moment fragmentation in spin ice. *Nat. Commun.* **2021**, *12*, 3047.
(19) Lefrancois, E.; Cathelin, V.; Lhotel, E.; Robert, J.; Lejay, P.; Colin, C. V.; Canals, B.; Damay, F.; Ollivier, J.; Fak, B.; et al. Fragmentation in spin ice from magnetic charge injection. *Nat. Commun.* **2017**, *8*, 209.
(20) Slobinsky, D.; Pili, L.; Baglietto, G.; Grigera, S. A.; Borzi, R. A. Monopole matter from magnetoelastic coupling in the Ising pyrochlore. *Commun. Phys.* **2021**, *4*, 56.
(21) Hao, L.; Yi, D.; Wang, M.; Liu, J.; Yu, P. Emergent quantum phenomena in atomically engineered iridate heterostructures. *Fundam. Res.* **2023**, *3*, 313−321.
(22) Narang, P.; Garcia, C. A. C.; Felser, C. The topology of electronic band structures. *Nat. Mater.* **2021**, *20*, 293−300.
(23) Kim, W. J.; Oh, T.; Song, J.; Ko, E. K.; Li, Y.; Mun, J.; Kim, B.; Son, J.; Yang, Z.; Kohama, Y.; et al. others Strain engineering of the magnetic multipole moments and anomalous Hall effect in pyrochlore iridate thin films. *Sci. Adv.* **2020**, *6*, No. eabb1539.
(24) Han, W.; Otani, Y.; Maekawa, S. Quantum materials for spin and charge conversion. *npj Quant. Mater.* **2018**, *3*, 27.
(25) Mi, M.; Xiao, H.; Yu, L.; Zhang, Y.; Wang, Y.; Cao, Q.; Wang, Y. Two-dimensional magnetic materials for spintronic devices. *Mater. Today Nano* **2023**, *24*, 100408.
(26) Li, Y.; Zhang, W.; Tyberkevych, V.; Kwok, W.-K.; Hoffmann, A.; Novosad, V. Hybrid magnonics: Physics, circuits, and applications for coherent information processing. *J. Appl. Phys.* **2020**, *128*, 130902.
(27) Jiang, Z.; Lim, J.; Li, Y.; Pfaff, W.; Lo, T.-H.; Qian, J.; Schleife, A.; Zuo, J.-M.; Novosad, V.; Hoffmann, A. Integrating magnons for quantum information. *Appl. Phys. Lett.* **2023**, *123*, 130501.
(28) Udagawa, M., Jaubert, L., Eds. *Spin Ice*; Springer, 2021.
(29) Morris, D. J. P.; Tennant, D. A.; Grigera, S. A.; Klemke, B.; Castelnovo, C.; Moessner, R.; Czternasty, C.; Meissner, M.; Rule, K. C.; Hoffmann, J.-U.; Kiefer, K.; Gerischer, S.; Slobinsky, D.; Perry, R. S. Dirac Strings and Magnetic Monopoles in the Spin Ice $Dy_2Ti_2O_7$. *Science* **2009**, *326*, 411−414.
(30) Hwang, K.; Kim, Y. B. Theory of Multifarious Quantum Phases and Large Anomalous Hall Effect in Pyrochlore Iridate Thin Films. *Sci. Rep.* **2016**, *6*, 30017.
(31) Hwang, K.; Trivedi, N.; Randeria, M. Topological magnons with nodal-line and triple-point degeneracies: Implications for thermal Hall effect in pyrochlore iridates. *Phys. Rev. Lett.* **2020**, *125*, 047203.
(32) Castelnovo, C.; Moessner, R.; Sondhi, S. L. Magnetic monopoles in spin ice. *Nature* **2008**, *451*, 42−45.
(33) Balents, L. Weyl electrons kiss. *Physics* **2011**, *4*, 36.
(34) Wan, X.; Turner, A. M.; Vishwanath, A.; Savrasov, S. Y. Topological semimetal and Fermi-arc surface states in the electronic structure of pyrochlore iridates. *Phys. Rev. B* **2011**, *83*, 205101.
(35) Go, A.; Witczak-Krempa, W.; Jeon, G. S.; Park, K.; Kim, Y. B. Correlation effects on 3d topological phases: From bulk to boundary. *Phys. Rev. Lett.* **2012**, *109*, 066401.
(36) Gallagher, J.; Esser, B.; Morrow, R.; Dunsiger, S.; Williams, R.; Woodward, P.; McComb, D.; Yang, F. Epitaxial growth of iridate pyrochlore $Nd_2Ir_2O_7$ films. *Sci. Rep.* **2016**, *6*, 22282.
(37) Fujita, T.; Kozuka, Y.; Uchida, M.; Tsukazaki, A.; Arima, T.-h.; Kawasaki, M. Odd-parity magnetoresistance in pyrochlore iridate thin films with broken time-reversal symmetry. *Sci. Rep.* **2015**, *5*, 9711.
(38) Bovo, L.; Rouleau, C. M.; Prabhakaran, D.; Bramwell, S. T. Layer-by-layer epitaxial thin films of the pyrochlore $Tb_2Ti_2O_7$. *Nanotechnology* **2017**, *28*, 055708.
(39) Wen, F.; Wu, T.-C.; Liu, X.; Terilli, M.; Kareev, M.; Chakhalian, J. Epitaxial stabilization of (111)-oriented frustrated quantum pyrochlore thin films. *J. Appl. Phys.* **2021**, *129*, 025302.
(40) Wen, F. *Correlated Electrons on Engineered Pyrochlore Lattices*; Ph.D. Thesis; Rutgers: Piscataway, NJ, 2022.
(41) Singh, S.; Bandyopadhyay, A. In *Pyrochlore Ceramics*; Chowdhury, A., Ed.; Elsevier, 2022; pp 25−94.
(42) Yang, W.; Xie, Y.; Zhu, W.; Park, K.; Chen, A.; Losovyj, Y.; Li, Z.; Liu, H.; Starr, M.; Acosta, J. A. Epitaxial thin films of pyrochlore iridate $Bi_{2+x}Ir_{2-y}O_{7-\delta}$: structure, defects and transport properties. *Sci. Rep.* **2017**, *7*, 7740.
(43) Guo, L.; Shang, S.-L.; Campbell, N.; Evans, P. G.; Rzchowski, M.; Liu, Z.-K.; Eom, C.-B. Searching for a route to synthesize in situ epitaxial $Pr_2Ir_2O_7$ thin films with thermodynamic methods. *npj Comput. Mater.* **2021**, *7*, 144.

https://doi.org/10.1021/acs.nanolett.4c03969
Nano Lett. 2025, 25, 966−972

(44) Rabinovich, K.; Kim, G.; Yaresko, A.; Christiani, G.; Logvenov, G.; Keimer, B.; Boris, A. Epitaxial growth and stoichiometry control of pyrochlore Nd 2 Ru 2 O 7 thin films. *Phys. Rev. Mater.* **2024**, *8*, 053801.
(45) Kim, W. J.; Ko, E. K.; Kim, S. Y.; Kim, B.; Noh, T. W. In-operando spectroscopic ellipsometry studies of IrO_2 dynamic instabilities: Guide to in-situ growth of pyrochlore iridate thin films. *Curr. Appl. Phys.* **2019**, *19*, 400−405.
(46) Song, J.; Ko, E. K.; Lee, S.; Mun, J.; Jeong, J. H.; Lee, J. H.; Kim, W. J.; Kim, M.; Li, Y.; Lee, J. H.; Noh, T. W. others Engineering structural homogeneity and magnetotransport in strained $Nd_2Ir_2O_7$ films. *APL Mater.* **2023**, *11*, 061104.
(47) Kim, W. J.; Song, J.; Li, Y.; Noh, T. W. Perspective on solid-phase epitaxy as a method for searching novel topological phases in pyrochlore iridate thin films. *APL Mater.* **2022**, *10*, 080901.
(48) Evans, P. G.; Chen, Y.; Tilka, J. A.; Babcock, S. E.; Kuech, T. F. Crystallization of amorphous complex oxides: New geometries and new compositions via solid phase epitaxy. *Curr. Opin. Solid State Mater. Sci.* **2018**, *22*, 229−242.
(49) Liu, X.; Wen, F.; Karapetrova, E.; Kim, J.-W.; Ryan, P.; Freeland, J.; Terilli, M.; Wu, T.-C.; Kareev, M.; Chakhalian, J. In-situ fabrication and transport properties of (111) $Y_2Ir_2O_7$ epitaxial thin film. *Appl. Phys. Lett.* **2020**, *117*, 041903.
(50) Liu, X.; Fang, S.; Fu, Y.; Ge, W.; Kareev, M.; Kim, J.-W.; Choi, Y.; Karapetrova, E.; Zhang, Q.; Gu, L.; et al. Magnetic Weyl semimetallic phase in thin films of $Eu_2Ir_2O_7$. *Phys. Rev. Lett.* **2021**, *127*, 277204.
(51) Jeong, Y.; Sakuraba, M.; Matsuura, T.; Murota, J. In *Rapid Thermal Processing for Future Semiconductor Devices*; Fukuda, H., Ed.; Elsevier Science: Amsterdam, 2003; pp 139−144.
(52) Zhou, W.-X.; Cheng, Y.; Chen, K.-Q.; Xie, G.; Wang, T.; Zhang, G. Thermal conductivity of amorphous materials. *Adv. Funct. Mater.* **2020**, *30*, 1903829.
(53) Che, J.; Wang, X.; Liu, X.; Liang, G.; Zhang, S. Thermal transport property in pyrochlore-type and fluorite-type $A_2B_2O_7$ oxides by molecular dynamics simulation. *Int. J. Heat Mass Transfer* **2022**, *182*, 122038.
(54) Ishibe, T.; Okuhata, R.; Kaneko, T.; Yoshiya, M.; Nakashima, S.; Ishida, A.; Nakamura, Y. Heat transport through propagon-phonon interaction in epitaxial amorphous-crystalline multilayers. *Commun. Phys.* **2021**, *4*, 153.
(55) Johnson, B. C.; McCallum, J. C.; Aziz, M. J. *Handbook of Crystal Growth*; Elsevier, 2015; pp 317−363.
(56) Marks, S. D.; Lin, L.; Zuo, P.; Strohbeen, P. J.; Jacobs, R.; Du, D.; Waldvogel, J. R.; Liu, R.; Savage, D. E.; Booske, J. H.; et al. Solid-phase epitaxial growth of the correlated-electron transparent conducting oxide $SrVO_3$. *Phys. Rev. Mater.* **2021**, *5*, 083402.
(57) Sambri, A.; Cristensen, D.; Trier, F.; Chen, Y.; Amoruso, S.; Pryds, N.; Bruzzese, R.; Wang, X. Plasma plume effects on the conductivity of amorphous-$LaAlO_3/SrTiO_3$ interfaces grown by pulsed laser deposition in O_2 and Ar. *Appl. Phys. Lett.* **2012**, *100*, 231605.
(58) Kareev, M.; Prosandeev, S.; Gray, B.; Liu, J.; Ryan, P.; Kareev, A.; Ju Moon, E.; Chakhalian, J. Sub-monolayer nucleation and growth of complex oxides at high supersaturation and rapid flux modulation. *J. Appl. Phys.* **2011**, *109*, 114303.
(59) Anderson, M. A.; El Baggari, I.; Brooks, C. M.; Powell, T.; Lygouras, C.; N'Diaye, A. T.; Koohpayeh, S. M.; Nordlander, J.; Mundy, J. A. Defect Engineering in Epitaxial Thin Films of the Pyrochlore Frustrated Magnet $Tb_2Ti_2O_7$. *Chem. Mater.* **2024**, *36*, 2325−2333.
(60) Cavagna, A. Supercooled liquids for pedestrians. *Phys. Rep.* **2009**, *476*, 51−124.
(61) Bolmatov, D.; Zav'yalov, D.; Zhernenkov, M.; Musaev, E. T.; Cai, Y. Q. Unified phonon-based approach to the thermodynamics of solid, liquid and gas states. *Ann. Phys.* **2015**, *363*, 221−242.
(62) Trachenko, K. *Theory of Liquids: From Excitations to Thermodynamics*; Cambridge University Press, 2023.
(63) Mostaed, A.; Balakrishnan, G.; Lees, M. R.; Yasui, Y.; Chang, L.-J.; Beanland, R. Atomic structure study of the pyrochlore $Yb_2Ti_2O_7$ and its relationship with low-temperature magnetic order. *Phys. Rev. B* **2017**, *95*, 094431.
(64) Ohno, M.; Fujita, T. C.; Kawasaki, M. Impact of iso-structural template layer on stabilizing pyrochlore $Bi_2Rh_2O_7$. *Appl. Phys. Lett.* **2023**, *122*, 251601.
(65) Zhang, H.; Xing, C.; Noordhoek, K.; Liu, Z.; Zhao, T.; Horak, L.; Huang, Q.; Hao, L.; Yang, J.; Pandey, S.; et al. Anomalous magnetoresistance by breaking ice rule in $Bi_2Ir_2O_7/Dy_2Ti_2O_7$ heterostructure. *Nat. Commun.* **2023**, *14*, 1404.
(66) Wu, T.-C.; Chang, Y.; Wu, A.-K.; Terilli, M.; Wen, F.; Kareev, M.; Choi, E. S.; Graf, D.; Zhang, Q.; Gu, L. Electronic anisotropy and rotational symmetry breaking at a Weyl semimetal/spin ice interface *arXiv Preprints* **2024**, arXiv:2409.18880 https://arxiv.org/abs/2409.18880.
(67) Turner, S. R.; Pailhes, S.; Bourdarot, F.; Ollivier, J.; Sidis, Y.; Castellan, J.-P.; Zanotti, J.-M.; Berrod, Q.; Porcher, F.; Bosak, A.; Feuerbacher, M.; Schober, H.; de Boissieu, M.; Giordano, V. M. Phonon behavior in a random solid solution: a lattice dynamics study on the high-entropy alloy FeCoCrMnNi. *Nat. Commun.* **2022**, *13*, 7509.
(68) Shapiro, M. C.; Riggs, S. C.; Stone, M. B.; de la Cruz, C. R.; Chi, S.; Podlesnyak, A. A.; Fisher, I. R. Structure and magnetic properties of the pyrochlore iridate $Y_2Ir_2O_7$. *Phys. Rev. B* **2012**, *85*, 214434.
(69) Ruminy, M.; Valdez, M. N.; Wehinger, B.; Bosak, A.; Adroja, D. T.; Stuhr, U.; Iida, K.; Kamazawa, K.; Pomjakushina, E.; Prabakharan, D.; et al. First-principles calculation and experimental investigation of lattice dynamics in the rare-earth pyrochlores $R_2Ti_2O_7$ (R = Tb, Dy, Ho). *Phys. Rev. B* **2016**, *93*, 214308.
(70) Li, C. W.; Smith, H. L.; Lan, T.; Niedziela, J. L.; Munoz, J. A.; Keith, J. B.; Mauger, L.; Abernathy, D. L.; Fultz, B. Phonon anharmonicity of monoclinic zirconia and yttrium-stabilized zirconia. *Phys. Rev. B* **2015**, *91*, 144302.

https://doi.org/10.1021/acs.nanolett.4c03969
Nano Lett. 2025, 25, 966−972